

Analytic approximations of neutrino luminosities and heat capacities of neutron stars with nucleon cores

D. D. Ofengeim^{1,3*}, M. Fortin², P. Haensel², D. G. Yakovlev³, J. L. Zdunik²

¹ *St Petersburg Academic University, Khlopina 8/3, St Petersburg 194021, Russia*

² *N. Copernicus Astronomical Center, Bartycka 18, 00-716 Warsaw, Poland*

³ *Ioffe Institute, Politekhnicheskaya 26, St Petersburg 194021, Russia*

Accepted . Received ; in original form

ABSTRACT

We derive analytic approximations of neutrino luminosities and heat capacities of neutron stars with nucleon cores valid for a wide class of equations of state of dense nucleon matter. The neutrino luminosities are approximated for the three cases in which they are produced by (i) direct Urca or (ii) modified Urca processes in non-superfluid matter, or (iii) neutrino-pair bremsstrahlung in neutron-neutron collisions (when other neutrino reactions are suppressed by strong proton superfluidity). The heat capacity is approximated for the two cases of (i) non-superfluid cores and (ii) the cores with strong proton superfluidity. The results can greatly simplify numerical simulations of cooling neutron stars with isothermal interiors at the neutrino and photon cooling stages as well as simulations of quasi-stationary internal thermal states of neutron stars in X-ray transients. For illustration, a model-independent analysis of thermal states of the latter sources is outlined.

Key words: dense matter – stars: neutron – neutrino emission – XRTs: quiescent.

1 INTRODUCTION

It is well known that observations of thermal radiation from cooling (isolated) neutron stars and from accreting neutron stars in quiescent states of X-ray transients (XRTs) can be used to infer (constrain) parameters of neutron stars and explore properties of superdense matter in their interiors (e.g., Yakovlev & Haensel 2003; Yakovlev et al. 2003; Yakovlev & Pethick 2004; Page et al. 2009; Potekhin et al. 2015 and references therein). This can be done by modeling thermal states and evolution of isolated and transiently accreting neutron stars and by comparing theoretical models with observations.

In this way one can test various model equations of state (EOSs) of superdense matter in neutron star cores — whether these EOSs are consistent with the data or not. Direct numerical modeling for the different EOSs and masses of neutron stars is often time consuming and requires complicated computer codes. It is the aim of the present paper to simplify the task by obtaining analytic approximations for basic integral properties of neutron stars which determine their thermal evolution.

Specifically, we consider thermally relaxed neutron stars which are isothermal inside (e.g. Glen & Sutherland 1980). Taking into account the effects of General Relativity, they should possess spacially constant redshifted internal temperature

$$\tilde{T} = T \exp \Phi, \quad (1)$$

where T is a local temperature of the matter and Φ is the metric function which determines gravitational redshift. A noticeable temperature gradient persists only in a thin outer (heat blanketing) envelope with a rather poor thermal conductivity; its thickness does not exceed a few hundred meters (e.g., Gudmundsson et al. 1983; Potekhin et al. 1997). We will study redshifted integrated neutrino luminosities L_ν^∞ and heat capacities C of such stars which are the main ingredients for simulating their thermal structure and evolution. These quantities are mainly determined by bulky and massive neutron star cores and depend on \tilde{T} . They depend also on the EOS of neutron star matter and on the stellar mass M . The neutrino luminosity L_ν^∞ is the sum of the luminosities provided by different neutrino emission mechanisms. Both quantities, L_ν^∞ and C , can be strongly affected by superfluidity in the neutron star cores.

We study a wide class of EOSs of neutron star cores composed of neutrons, protons, electrons and muons. These EOSs may open or forbid the powerful direct Urca processes of neutrino emission in neutron star cores (Lattimer et al. 1991). We consider either non-superfluid (normal) cores or the cores with strong proton superfluidity which suppresses all neutrino processes involving protons as well as the proton heat capacity in the core (e.g. Yakovlev et al. 2001). We will calculate L_ν^∞ and $C \approx C_{\text{core}}$ and approximate them by analytic expressions which are universal for all chosen EOSs. This universality greatly simplifies theoretical analysis of observational data on cooling isolated and transiently accreting neutron stars. For illustration, we give a sketch of such an analysis for quasi-stationary neutron stars in XRTs. In our analysis we neglect possible effects of magnetic fields.

* E-mail: ddofengeim@gmail.com

2 COOLING PROPERTIES OF NEUTRON STARS

Let us outline the main elements of the cooling theory of neutron stars (e.g., Yakovlev & Pethick 2004). During the first $\sim 10^5$ yr after their birth neutron stars cool mostly via neutrino emission from their interiors. During an initial cooling period $\sim 10 - 100$ yr the internal regions of the star become isothermal. Since then neutrinos are mainly generated in the stellar core. The basic neutrino emission mechanisms in the core are the *direct Urca* (DU) and *modified Urca* (MU) processes as well as *neutrino-pair bremsstrahlung in baryon collisions*. Neutrino emissivities of these processes strongly depend on the properties of the matter — on composition and superfluidity of baryons (e.g. Yakovlev et al. 2001).

In the present paper we assume that the neutron star core consists of neutrons with some admixtures of protons, electrons and muons (*npeμ*-matter) in beta equilibrium. The neutrino emissivities of relevant processes are reviewed, for instance, by Yakovlev et al. (2001). We will study the case of fully non-superfluid (non-SF) matter and the case of strongly superfluid (SF) protons with other particles being in normal states. The first case refers to the standard neutrino emission level and describes the so called standard neutrino candles. The main contribution to the luminosity of the neutron star core comes from the DU or MU processes. For the MU process, we have

$$Q_{\text{MU}} = Q_{\text{MU}0} \left(\frac{n_p}{n_0} \right)^{1/3} T_9^8 \Omega(n_n, n_p, n_e, n_\mu), \quad (2)$$

where n_n , n_p , n_e and n_μ are the number densities of neutrons, protons, electrons and muons, respectively; $n_0 = 0.16 \text{ fm}^{-3}$ is the standard number density of nucleons in saturated nuclear matter, T_9 is a local temperature expressed in 10^9 K and $\Omega \sim 1$ is a dimensionless factor to account for different branches of the process (see, e.g., Yakovlev et al. 2001; Kaminker et al. 2016). In this work we need only the main dependence $Q_{\text{MU}} \propto n_p^{1/3}$. The factor $Q_{\text{MU}0} \approx 1.75 \times 10^{21} \text{ erg cm}^{-3} \text{ s}^{-1}$ is calculated under the assumptions described by Yakovlev et al. (2001), with an effective masses of protons and neutrons $m_p^* = 0.7m_p$ and $m_n^* = 0.7m_n$, respectively.

For the DU process, we have (e.g., Yakovlev et al. 2001)

$$Q_{\text{DU}} = Q_{\text{DU}0} \left(\frac{n_e}{n_0} \right)^{1/3} T_9^6 (\Theta_{\text{npe}} + \Theta_{\text{n}\mu}), \quad (3)$$

where $Q_{\text{DU}0} \approx 1.96 \times 10^{27} \text{ erg cm}^{-3} \text{ s}^{-1}$, while the factors Θ_{npe} and $\Theta_{\text{n}\mu}$ are equal to 1 (open the electron and muon processes, respectively) if Fermi momenta of reacting particles satisfy the triangle condition; otherwise, these factors are zero. Because of the triangle conditions, the electron and muon DU processes have thresholds and can operate only in the central regions of massive neutron stars. For some EOSs, they do not operate at all.

The SF case corresponds to the most slowly cooling neutron stars (e.g., Ofengeim et al. 2015), where all neutrino reactions involving protons are strongly suppressed by proton superfluidity and the most efficient neutrino emission is provided by the nn-bremsstrahlung. Then (e.g. Yakovlev et al. 2001)

$$Q_{\text{nn}} = Q_{\text{nn}0} \left(\frac{n_n}{n_0} \right)^{1/3} T_9^8, \quad (4)$$

where $Q_{\text{nn}0} \approx 1.77 \times 10^{19} \text{ erg cm}^{-3} \text{ s}^{-1}$.

Another quantity important for cooling neutron stars is the specific heat of the neutron core c_{core} . Since neutron stars are mainly composed of strongly degenerate particles, the heat capacities at constant volume and pressure are almost identical and we do not

Table 1. The basic parameters of stars with the selected EOSs; M_{max} and R_{min} refer to most massive stable stars; M_{DU} and R_{DU} refer to stars where the DU process becomes allowed.

EOS	M_{max}, M_\odot	$R_{\text{min}}, \text{km}$	M_{DU}, M_\odot	R_{DU}, km
NL3 $\omega\rho$	2.75	13.00	2.60	13.79
PAL4-240	1.93	10.24	1.64	11.93
BSk21	2.27	11.01	1.59	12.59
BSk20	2.16	10.10	—	—
SLy	2.05	9.90	—	—
APR II	1.92	10.20	1.89	10.83
APR IV	2.16	10.82	1.73	12.48
DDME2	2.48	12.05	—	—

discriminate between them. In the non-SF case there are four contributions to the specific heat in a nucleon neutron star core,

$$c_{\text{core}} = c_n + c_p + c_e + c_\mu. \quad (5)$$

For $a = n, p, e, \mu$ one has

$$c_a = \frac{k_B^2}{3\hbar^3} T m_a^* p_{Fa}, \quad (6)$$

where k_B is the Boltzmann constant while m_a^* and p_{Fa} are, respectively, the effective mass and the Fermi momentum of particles a . Note that the main contributions to c_{core} comes from c_n and c_p (e.g., Page 1993). Taking $m_n^* = 0.7m_n$ and $m_p^* = 0.7m_p$, we obtain

$$c_N \approx c_0 \left(\frac{n_N}{n_0} \right)^{1/3} T_9, \quad (7)$$

with $N = n$ or p , and $c_0 = 1.12 \times 10^{20} \text{ erg cm}^{-3} \text{ K}^{-1}$. In the case of very strong proton superfluidity one has $c_p \rightarrow 0$.

Integration of Q and c_{core} over the neutron star core gives the neutrino luminosity L_ν and the heat capacity C_{core} of the core. The same quantities for the crust are negligible after the star reaches the state of internal thermal relaxation (e.g. Yakovlev et al. 2001; Yakovlev & Pethick 2004). If so, L_ν and C_{core} are almost equal to the total neutrino luminosity and heat capacity of the star, respectively. We will perform the integration of Q and c_{core} for different EOSs in the core assuming isothermal interior of the star.

3 ZOO OF EQUATIONS OF STATE

Let us take eight EOSs of superdense matter in neutron star cores. They are illustrated in Figs. 1–3. The NL3 $\omega\rho$ and DDME2 EOSs are described in Fortin et al. (2016) and in references therein; the SLy EOS is taken from Douchin & Haensel (2001); PAL4-240 is the model after Page & Applegate (1992) but with a different compression modulus at saturation, $K_0 = 240 \text{ MeV}$ (see also the PAL model in the Appendix D of Haensel et al. 2007); the APR II EOS is introduced by Gusakov et al. (2005); the BSk20 and BSk21 EOSs are parametrized by Potekhin et al. (2013), and the APR IV EOS is constructed by Kaminker et al. (2014) (who called it the HHJ EOS). For the SLy, BSk20 and BSk21 models, the EOSs in the crust and the core are calculated in a unified way; the NL3 $\omega\rho$ and DDME2 crustal parts are described by Fortin et al. (2016); for other models, the smooth composition EOS of the crust (Haensel et al. 2007) is used. The most important parameters of neutron stars for the selected EOSs are listed in Table 1.

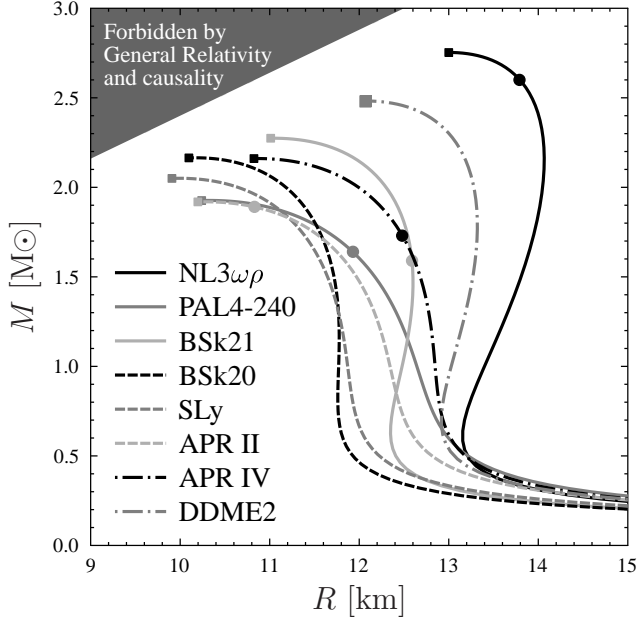


Figure 1. $M - R$ relations for the selected EOSs. Filled squares mark maximum masses of stable neutron stars with respective EOSs; filled circles mark minimum masses of stars where DU process is open.

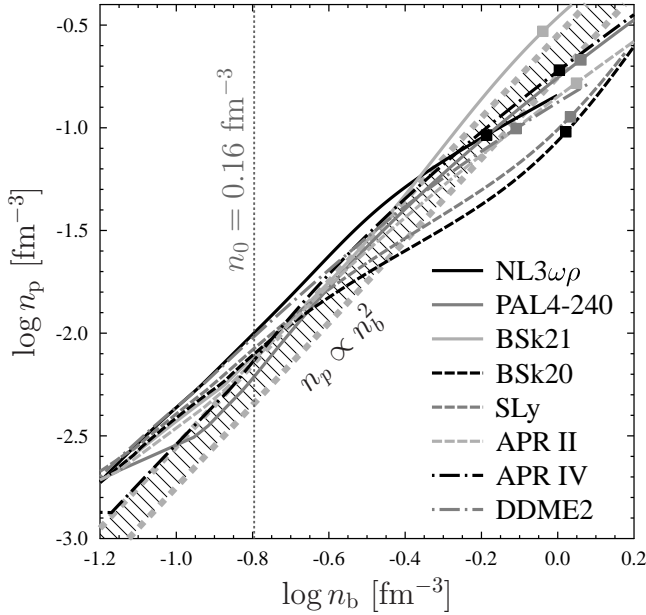


Figure 3. $n_p - n_b$ relations for the selected EOSs. Squares mark the maximum n_b which is possible in stable neutron stars with corresponding EOSs. The thick shaded strip corresponds to the models which are similar to the free-particle model. See text for details.

The $M(R)$ relations for neutron star models with these EOSs are plotted in Fig. 1. We choose the EOSs with different stiffness in order to consequently cover a large part of the $M - R$ plane. Squares in Fig. 1 correspond to the most massive stable neutron star models. The selected EOSs are reasonably consistent with recent discoveries of two massive ($M \approx 2 M_\odot$) neutron stars (Demorest et al. 2010; Antoniadis et al. 2013). Circles mark configurations where

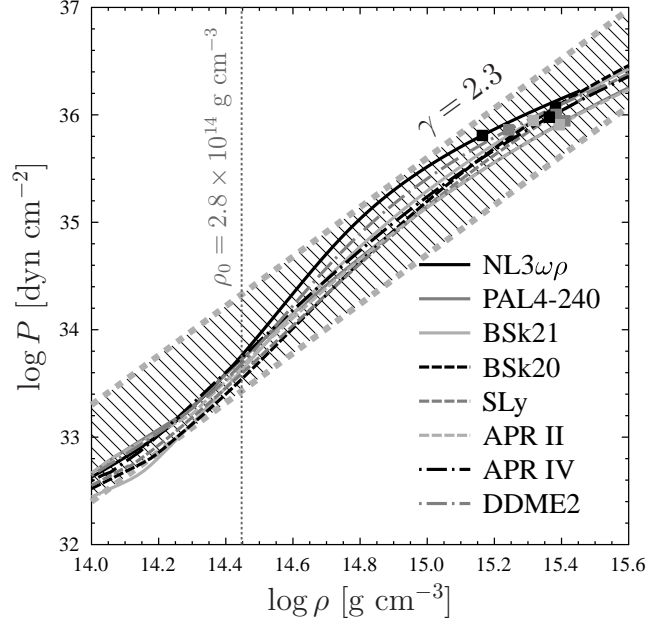


Figure 2. $P - \rho$ relations for the selected EOSs. Squares mark the maximum central densities of stable neutron stars with respective EOSs. The thick shaded strip shows a family of polytropic EOSs with $P \propto \rho^\gamma$, where $\gamma = 2.3$ is the overall mean value. See text for details.

the DU process becomes allowed. Only five EOSs from Table 1 open the DU process before the most massive stable configuration is reached.

In Fig. 2 we plot the $P - \rho$ relations for the selected EOSs. These relations have several common features. First, the EOSs at $\rho \sim \rho_0 = 2.8 \times 10^{14} \text{ g cm}^{-3}$ (the dotted vertical line) are not dramatically different (differences in P are within a factor of 2). It is because, as a rule, the EOSs are constructed in such a way to reproduce the properties of saturated nuclear matter which are well studied in laboratory. Secondly, the stiffer the high-density EOS, the larger M_{max} . Finally, in spite of the similarity of the $P - \rho$ relations near ρ_0 they are sufficiently different at $\rho \gtrsim 2\rho_0$ which results in rather different $M - R$ relations. The straight thick shaded strip line in Fig. 2 corresponds to a family of simple polytropic EOS models $P \propto \rho^\gamma$ with the power-law index $\gamma = 2.3$. It is a good overall approximation as discussed in Section 4.3.

Fig. 3 illustrates another important property of the selected EOSs, the relation between the proton n_p and total baryon n_b number densities. A bunch of the curves for the different EOSs is the thinnest at $n_b \sim n_0$ (the dotted vertical line). It is a consequence of the calibration of the EOSs to the standard nuclear theory. The straight thick shaded strip corresponds to the relations $n_p \propto n_b^2$, which can be derived from the free-particle model at not too high n_b (e.g., Friman & Maxwell 1979; Shapiro & Teukolsky 1983). Fig. 3 shows that this simple approximation is qualitatively accurate which is sufficient for our analysis.

Let us stress that we do not intend to accurately fit the EOSs or number densities of different particles. Our aim is to suggest some simple scaling expressions for these quantities and use them to fit the expressions for the integral quantities, such as C_{core} and L_ν^∞ . One can treat these scaling expressions as purely auxiliary and phenomenological (although we prefer to introduce them on physical grounds). We will see that the integration over the core absorbs

the inaccuracy of scaling expressions and enables us to accurately describe the integral quantities.

4 INTEGRATION OF NEUTRINO LUMINOSITY AND HEAT CAPACITY

4.1 Basic expressions

The neutrino luminosity L_ν^∞ of a neutron star core redshifted for a distant observer is given by

$$L_\nu^\infty = \int_0^{R_{\text{core}}} Q(\rho, T) \exp(2\Phi) \frac{4\pi r^2 dr}{\sqrt{1 - 2Gm/(rc^2)}}. \quad (8)$$

The heat capacity of the core is

$$C_{\text{core}} = \int_0^{R_{\text{core}}} c_{\text{core}}(\rho, T) \frac{4\pi r^2 dr}{\sqrt{1 - 2Gm/(rc^2)}}. \quad (9)$$

Here R_{core} is the core radius, $m = m(r)$ is the gravitational mass inside the sphere of radial coordinate r , and $\Phi(r)$ is the metric function determined by the equation (e.g. Haensel et al. 2007, Ch. 6)

$$\frac{d\Phi}{dr} = -\frac{1}{P + \rho c^2} \frac{dP}{dr}. \quad (10)$$

The neutrino emissivity and the specific heat are expressed here as functions of the local temperature T and the local density ρ . In a star with isothermal interiors $T(r)$ is given by equation (1), $T = \tilde{T} \exp(-\Phi)$, with \tilde{T} being constant over the isothermal region.

Let us analyse three cases of neutrino emission in equation (8). The first is the SF case, where $Q = Q_{\text{nn}}$ is given by equation (4). The second is the non-SF case with the forbidden DU process, so that $Q = Q_{\text{MU}}$, equation (2). The third case is also for the non-SF core but with the allowed DU process. In this case, we set $Q = Q_{\text{DU}}$, given by equation (3). To simplify our analysis, in this paper we use $Q = Q_{\text{DU}}$ throughout the entire neutron star core (to avoid complications associated with the introduction of the DU threshold). This simplification is qualitatively justified because, typically, $Q_{\text{DU}} \sim 10^6 Q_{\text{MU}}$, and even a small central kernel with the allowed DU process makes $L_{\nu\text{DU}}^\infty$ drastically larger than $L_{\nu\text{MU}}^\infty$. However, it somewhat overestimates $L_{\nu\text{DU}}^\infty$ and gives only its firm upper limit.

As far as the specific heat is concerned, we consider two cases, the non-SF and SF ones. They differ only by the presence or absence of c_p . Equations (8) and (9) allow us to numerically integrate L_ν^∞ and C_{core} in the indicated cases for the selected EOSs.

4.2 Analytic approximations of the integrals

Exact analytic integration in equations (8) and (9) is not possible. Instead, we derive approximate expressions for these integrals and calibrate them using the results of numerical integration.

Because the mass of a neutron star crust is typically about 1 per cent of the total mass M , we can safely set that $m(R_{\text{core}}) = M$ and $\Phi(R_{\text{core}}) = \Phi_{\text{surf}}$, where

$$\Phi_{\text{surf}} = \ln \sqrt{1 - x_g}, \quad x_g \equiv \frac{2GM}{Rc^2}. \quad (11)$$

It is convenient to introduce $\tilde{\Phi} = \Phi - \Phi_{\text{surf}}$.

To proceed further we need approximate expressions for the number densities of particles in neutron star cores. Let us assume that the main contribution to the baryon number density $n_b = n_n +$

n_p is provided by neutrons, and the number densities of charged particles are described by the model similar to the free-particle one,

$$n_n \approx n_b, \quad n_p \approx n_e \approx a n_0 \left(\frac{n_b}{n_0} \right)^2. \quad (12)$$

Here a is a dimensionless constant which can be treated as a value averaged over the all selected EOSs. The $n_b - \rho$ relation can be taken from Haensel et al. (2007, Ch. 6),

$$n_b = \frac{\rho}{m_0} \left(1 + \frac{P}{\rho c^2} \right) \exp \tilde{\Phi}; \quad (13)$$

m_0 being the rest mass per baryon in the ^{56}Fe nucleus.

The approximate equality $n_e \approx n_p$ in equation (12) can be significantly violated at very high densities where $n_\mu \sim n_e$. Such densities occur near the centers of massive neutron stars; their contribution to the integrated neutrino luminosities and heat capacities is small, except for $L_{\nu\text{DU}}$, where the contributions of the muon and electron DU processes are equal.

As mentioned above, we study the three scenarios (nn, MU and DU) of neutrino emission in equation (8). In the first (nn) case we take $Q = Q_{\text{nn}}$ from equation (4). In the second (MU) case we employ Q_{MU} from equation (2), but we will additionally simplify it assuming $\Omega(n_{n,p,e,\mu}) = \text{const}$. In the third (DU) case we use equation (3) but replace the sum of Θ -functions by a factor 2. Since typical densities, where the DU processes operate, are so high that muons appear, such a simplification is reasonable.

Considering the specific heat, we use the approximation (7), $c_{\text{core}} = b c_n$, with different constants b for the non-SF and SF cases.

Let us factorize (8) and (9) into dimensional and dimensionless terms. It is convenient to define

$$r = R_{\text{core}} x, \quad 0 < x < 1; \quad (14a)$$

$$\rho(r) = \frac{M}{R_{\text{core}}^3} f(x), \quad f(0) \sim 1, \quad f(1) \ll 1; \quad (14b)$$

$$m(r) = M F(x), \quad F(x) = 4\pi \int_0^x f(x') x'^2 dx'. \quad (14c)$$

We assume that $f(x)$ has a universal form for any EOS, M and R of our study. According to Lattimer & Prakash (2001), such an approximation is reasonable. Then equation (8) yields

$$L_\nu^\infty = a' \left(\frac{R_{\text{core}}}{R} \right)^3 Q_0 R^3 x_p^{k/3} \tilde{T}_9^n (1 - x_g)^{1-n/2} \times \int_0^1 x^2 dx \left[f(x) \left(1 + \frac{P}{\rho c^2} \right) \right]^{k/3} \times \exp \left[\left[\frac{k}{3} + 2 - n \right] \tilde{\Phi} \right] \left[1 - x_g \frac{R}{R_{\text{core}}} \frac{F(x)}{x} \right]^{-1/2}, \quad (15)$$

where $x_p = M/(\rho_0 R^3)$; $k = 1$, $n = 8$ and $Q_0 = Q_{\text{nn}0}$ for the nn-bremsstrahlung; $k = 2$, $n = 8$ and $Q_0 = Q_{\text{MU}0}$ for the MU process; $k = 2$, $n = 6$ and $Q_0 = Q_{\text{DU}0}$ for the DU process; In equation (15) we have introduced a dimensionless constant a' to absorb the inaccuracy of L_ν^∞ due to our approximations of $n_p(n_b)$ and Ω in the DU and MU cases; in the SF case $a' = 1$. Similarly, for the heat

capacity (9) we obtain

$$C_{\text{core}} = b' \left(\frac{R_{\text{core}}}{R} \right)^3 c_0 R^3 x_p^{1/3} \tilde{T}_9 (1 - x_g)^{-1/2} \times \int_0^1 x^2 dx \left[f(x) \left(1 + \frac{P}{\rho c^2} \right) \right]^{1/3} \times \exp \left(-\frac{2}{3} \tilde{\Phi} \right) \left[1 - x_g \frac{R}{R_{\text{core}}} \frac{F(x)}{x} \right]^{-1/2}, \quad (16)$$

where constants b' are different in the SF and non-SF cases.

Next consider a polytropic EOS, $P = P_0 (\rho/\rho_0)^\gamma$, with some effective γ whose value will be obtained later by calibrating to numerical calculations of L_ν^∞ and C_{core} . Then we analytically derive $\tilde{\Phi}$ from equation (10) with the condition $\tilde{\Phi}(R_{\text{core}}) = 0$,

$$\tilde{\Phi} = -\frac{\gamma}{\gamma - 1} \left[\ln \left(1 + \frac{P}{\rho c^2} \right) - \ln \left(1 + \frac{P_{\text{cc}}}{\rho_{\text{cc}} c^2} \right) \right], \quad (17)$$

where $\rho_{\text{cc}} = \rho(R_{\text{core}}) \approx \rho_0/2$ and $P_{\text{cc}} = P(\rho_{\text{cc}})$ are, respectively, the density and pressure at the core-crust interface. Actually, this solution behaves as

$$\exp \tilde{\Phi} \propto \left(1 + \frac{P}{\rho c^2} \right)^{-\gamma/(\gamma-1)}. \quad (18)$$

At the next step we stress that the ratio $R_{\text{core}}/R = 0.8 - 1.0$ only slightly varies for different stellar masses higher than 1 M_\odot . Thus we assume $R_{\text{core}}/R \approx 0.9$ to be constant in Eqs. (15) and (16). Then, combining equations (14b) and (18) with (15) and (16), we see that the integrals are parametrised by M and R . All uncertainties of calculations of the integrals are encapsulated in the functions $f(x)$ and $F(x)$. These functions should be smooth as proven by (14). Thus the dependence of the integrals in equations (15) and (16) on M and R can be understood using the midpoint method, by taking the integrands at some fixed value of x between 0 and 1, x_{mid} . For simplicity, we assume that this value is independent of M and R . It is convenient to introduce

$$J_{kp}(M, R) = a_1 x_p^{k/3} (1 - x_g)^{-p/2} \frac{(1 + a_3 x_p^{\gamma-1})^{\frac{p\gamma-k/3}{\gamma-1}}}{\sqrt{1 - a_2 x_g}}. \quad (19)$$

Then the final expressions for the neutrino luminosity and heat capacity take the forms

$$\left\{ \begin{array}{c} L_\nu^\infty \\ C_{\text{core}} \end{array} \right\} = \left\{ \begin{array}{c} Q_0 \\ c_0 \end{array} \right\} R^3 \tilde{T}_9^n J_{kp}(M, R). \quad (20)$$

Here we use R^3 instead of R_{core}^3 because R_{core}/R is taken to be constant in our analytic models and the difference is absorbed in fit parameters described below. The exponents n , p and k are taken from equations (15) and (16) and listed in Table 2. The dimensionless parameters a_1 , a_2 , a_3 and the most suitable values of γ in (19) will be obtained by the calibration to numerical calculations.

4.3 Calibration to numerical calculations

The integrals (8) and (9) have been calculated numerically. In this way we have obtained accurate values of L_ν^∞ and C_{core} for any selected EOS, any scenario (nn, MU, DU, SF, non-SF) and for a range of masses $M = 1.0 \text{ M}_\odot, 1.1 \text{ M}_\odot, \dots, M_{\text{max}}$. In the calculations, we have used the expressions for Q and c_{core} described in Sections 2 and 4.1. As mentioned above, while calculating $L_{\nu\text{DU}}^\infty$ we have extended Q_{DU} over the entire neutron star core. However, for the DU case we have not used stellar models with $M < 1.5 \text{ M}_\odot$ because $M_{\text{DU}} > 1.5 \text{ M}_\odot$ for all our models (Table 1).

Our numerical results are shown by different symbols in Fig. 4. These data have been used to calibrate our analytic approximation (20). We have obtained 109 values of the neutrino luminosity (cases nn and MU, excluding DU) as well as 109 values of the heat capacity (cases SF and non-SF). For the DU case we have excluded 40 values with $M < 1.5 \text{ M}_\odot$. The trial functions $L_\nu^\infty(M, R)$ and $C_{\text{core}}(M, R)$ (equations (19), (20)) have been calibrated to these data sets. The target function to minimize has been the relative root mean square (rms) error. The optimised values of a_1 , a_2 , a_3 and γ as well as the corresponding fit errors are listed in Table 2. The obtained approximations are also plotted on Fig. 4.

Let us discuss the approximations of L_ν^∞ . They are most precise for the nn-bremsstrahlung; the rms errors appear the smallest because Q_{nn} is independent of the fractions of charged particles in dense matter. However, it has large maximal relative error which occurs for the most massive star with the NL3 $\omega\rho$ EOS. This is because the approximation of this EOS by a single polytrope does not reproduce well its high density behaviour. The largest errors occur for the MU case due to a strong dependence of Q_{MU} on the fractions of charged particles through the factor Ω . The approximation of $L_{\nu\text{DU}}^\infty$ is more accurate than the approximation of $L_{\nu\text{MU}}^\infty$ because Q_{DU} depends on n_e in a rather simple way.

The importance of charged particle fractions can be demonstrated by instructive examples of the BSk20 and APR IV EOSs. In Figs. 1–4 the corresponding curves are plotted by short-dashed (BSk20) and dot-dashed (APR IV) lines. The initial numerical data in Fig. 4 are displayed by black squares (BSk20) and triangles (APR IV). According to Fig. 1, these EOSs have very close maximum masses, but the stars with the BSk20 EOS are more compact, i.e. have smaller radii than the APR IV stars of the same M . Roughly speaking, the $M - R$ relations for these EOSs differ by a shift along the R axis. This means that a BSk20 star is denser than an APR IV star, and, therefore, has larger L_ν^∞ . This is true for $L_{\nu\text{nn}}^\infty$ (Fig. 4): black squares (for BSk20) lie higher than black triangles (for APR IV). This feature is well reproduced by the black dashed and dot-dashed lines, which show the approximation (20) for these EOSs. In contrast, the MU and DU luminosities are sensitive to the $n_p - n_b$ relations. According to Fig. 3, the values of n_p for the APR IV EOS are noticeably higher than for the BSk20 EOS. The opposite effects of the two factors, the greater compactness of the BSk20 stars and the larger n_p for the APR IV stars, leads to their compensation. Accordingly, the DU as well as the MU neutrino luminosities for these EOSs appear to be close enough (triangles and black squares on the left-hand panel of Fig. 4 overlap). Because the approximation (20) is derived using not very accurate description of proton, electron and muon fractions, it cannot reproduce this effect exactly; an approximate expression gives $L_{\nu\text{DU}}^\infty$ and $L_{\nu\text{MU}}^\infty$ higher than numerical values for the BSk20 EOS and lower than for the APR IV EOS.

Another interesting note is that the parameter a_1 of our approximation takes very close values for the non-SF (DU and MU) cases but is several times larger for the SF (nn-bremsstrahlung) case. This is because a_1 should include the value $a^{1/3}$ from (12) and the extra factor $f^{1/3}(x_{\text{mid}})$ in the non-SF case but not in the SF case. Because both these factors are smaller than 1, the value of a_1 should be several times lower in the non-SF case than in the SF case, in agreement with Table 2.

Now let us outline the approximations of the heat capacity (the right-hand side of Fig. 4). The different EOSs give so close values of C_{core} , that the approximation (20) hardly resolves them. Note that the parameters a_2 , a_3 and γ , which determine the $C_{\text{core}} - M$ relation, are similar in the SF and non-SF cases. This supports the idea that

Table 2. Parameters of the approximations (19) and (20) for the neutrino luminosity L_ν^∞ and the heat capacity C_{core} . For the luminosity, ‘nn’ refers to the nn-bremsstrahlung (SF case), while ‘MU’ and ‘DU’ correspond to the MU and DU processes (non-SF case), respectively. For the heat capacity, the non-SF and SF cases differ by the presence or absence of the proton contribution. The two last columns give root-mean-square (rms) relative errors and maximal relative errors (indicating an EOS at which they occur, that always happens at $M = M_{\text{max}}$). See the text for details.

L_ν^∞ or C_{core}	Case	Q_0 or c_0	n	k	p	a_1	a_2	a_3	γ	rms	max error
L_ν^∞	nn (SF)	$1.77 \times 10^{19} \text{ erg cm}^{-3} \text{ s}^{-1}$	8	1	6	2.03	1.14	0.0047	2.51	0.14	0.54 at NL3 $\omega\rho$
	MU (non-SF)	$1.75 \times 10^{21} \text{ erg cm}^{-3} \text{ s}^{-1}$	8	2	6	1.12	1.14	0.0060	2.45	0.25	0.66 at NL3 $\omega\rho$
	DU (non-SF)	$1.96 \times 10^{27} \text{ erg cm}^{-3} \text{ s}^{-1}$	6	2	4	1.01	1.14	0.0031	2.48	0.16	0.40 at NL3 $\omega\rho$
C_{core}	non-SF	$1.12 \times 10^{20} \text{ erg cm}^{-3} \text{ K}^{-1}$	1	1	1	2.68	1.14	0.0174	2.11	0.05	0.12 at BSk20
	SF	$1.12 \times 10^{20} \text{ erg cm}^{-3} \text{ K}^{-1}$	1	1	1	2.01	1.06	0.0159	2.18	0.05	0.09 at NL3 $\omega\rho$

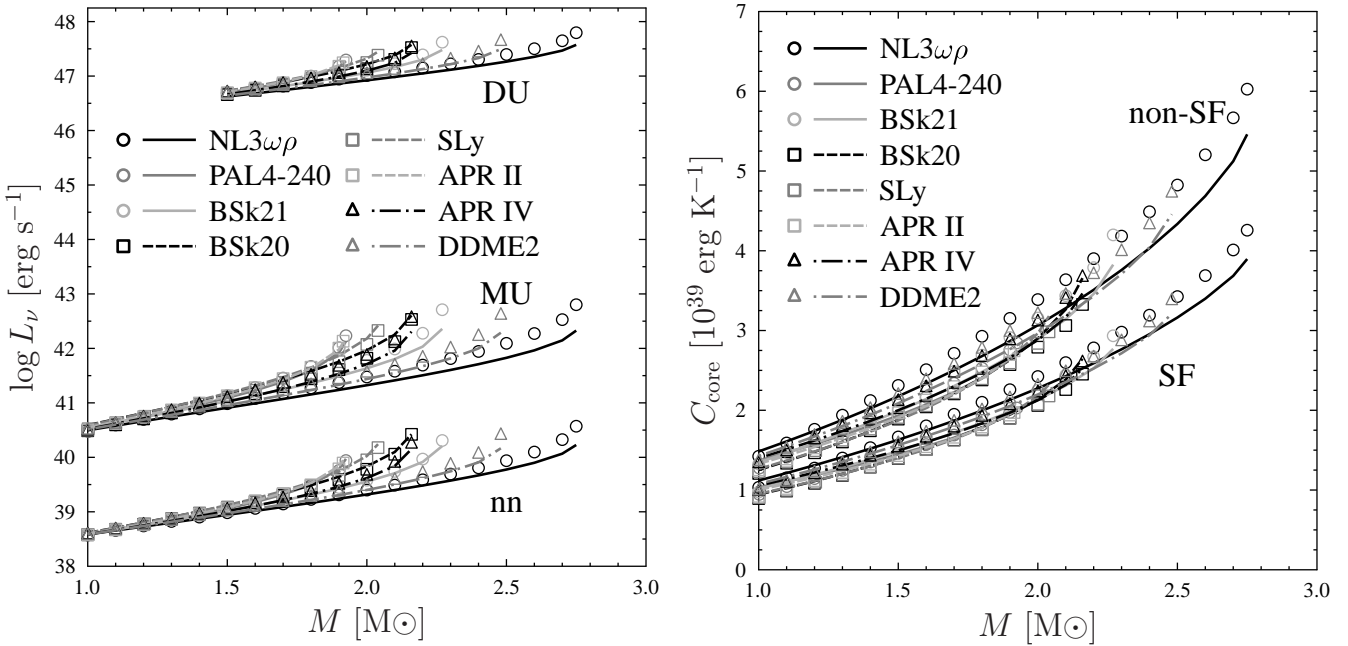


Figure 4. $L_\nu^\infty - M$ (left-hand panel) and $C_{\text{core}} - M$ (right-hand panel) relations for the seven selected EOSs at $\tilde{T} = 10^9 \text{ K}$. Lines show the approximation (20); squares, circles and triangles present numerical calculations. The labels ‘nn’, ‘MU’, ‘DU’, ‘SF’ and ‘non-SF’ are the same as in Table 2. For $L_{\nu\text{DU}}^\infty$, the DU process is artificially extended over the entire core, but the calculations are performed only at $M \geq 1.5 M_\odot$.

the behavior of the total specific heat is similar to that of c_n in both these cases. A difference between the values of a_1 shows that switching off the proton contribution by superfluidity just reduces the heat capacity by about 25 per cent, in agreement with the results by Page (1993).

Let us mention several common features of our approximations. First, we can see that the index γ ranges from about 2.1 to 2.5 with the average value $\gamma \approx 2.3$. Such a polytropic EOS is plotted in Fig. 2 by a thick green line and is in good agreement with the selected EOSs. Secondly, the largest errors occur at the maximum neutron star masses, because the higher the density the stronger the difference between the EOS models. Thirdly, the fact that the maximum errors occur for the NL3 $\omega\rho$ and BSk20 EOSs is explained by the largest deviations of $P - \rho$ (NL3 $\omega\rho$) and $n_p - n_b$ (BSk20) relations from the average trend (Fig. 3).

It is also remarkable that at low M the exact $L_\nu^\infty - M$ dependence is insensitive to an EOS. This gives hope to derive this dependence analytically for $M \lesssim 1.5 M_\odot$ which is out of the scope of the present work.

5 QUIESCENT STATES OF XRTS

For illustration, we apply our approximations of L_ν^∞ to analyse transiently accreting neutron stars in XRTs (low-mass X-ray binaries). The formalism of applying the neutron star cooling theory for exploring quasi-stationary thermal states of such objects in quiescence is well known (e.g. Yakovlev et al. 2003; Levenfish & Haensel 2007, also see Yakovlev & Pethick 2004). We will show that our approximations of L_ν^∞ simplify an analysis of observations.

5.1 Formalism of thermal states

Let us outline the main features of thermal quasi-stationary equilibrium of neutron stars in XRTs. During active states of such a source, the neutron star accretes from its low-mass companion. The accreted matter is compressed under the weight of newly accreted material. It looks as if the accreted matter sinks into deeper layers of the neutron star crust. This initiates nuclear transformations of the accreted matter accompanied by the deep crustal heating

(Haensel & Zdunik 1990, 2003, 2008) with the energy release of about 1.5 MeV per one accreted nucleon distributed mainly in the inner crust. This deep crustal heating can be sufficiently strong to warm up old transiently accreting stars and support their observable thermal radiation during quiescent states of XRTs (Brown et al. 1998).

We will not consider the episodes of rather long or intense accretion when the deep heating is too intense and destroys thermal equilibrium between the crust and the core (e.g. Degenaar et al. 2015 and references therein). We will restrict our analysis to weaker or shorter accretion episodes. Then the stellar interior remains isothermal and quasi-stationary. On average, this heating is balanced by the thermal emission of photons from the stellar surface and neutrinos from the stellar interior. In an observer rest frame one has the thermal balance of the form

$$L_\gamma^\infty + L_\nu^\infty = L_{\text{DCH}}^\infty, \quad (21)$$

where

$$L_\gamma^\infty = 4\pi\sigma R^2 T_s^4 (1 - x_g) \quad (22)$$

is the redshifted photon luminosity of the star as a function of the local effective surface temperature T_s , R and M (x_g is defined in equation (11)), L_ν^∞ is the neutrino luminosity (8) approximated by equation (20), and

$$L_{\text{DCH}}^\infty = L_{\text{DCH}}^{(0)} \langle \dot{M}_{10} \rangle \sqrt{1 - x_g} \quad (23)$$

is the integrated rate of the energy release due to deep crustal heating. The mass accretion rate $\langle \dot{M}_{10} \rangle = \langle \dot{M} \rangle / (10^{-10} \text{ M}_\odot \text{ yr}^{-1})$ has to be averaged over the neutron star cooling time scales, and $L_{\text{DCH}}^{(0)} = 9.2 \times 10^{33} \text{ erg s}^{-1}$ is consistent with the deep crustal heating rate (1.5 MeV per nucleon) given above.

Using equations (21)–(23) one can calculate and plot the neutron star heating curves in the $L_\gamma^\infty - \langle \dot{M} \rangle$ plane (e.g., Yakovlev & Pethick 2004; Levenfish & Haensel 2007). Here we consider the two limiting cases: (i) the photon cooling regime at $L_\gamma^\infty \gg L_\nu^\infty$ and (ii) the neutrino cooling regime at $L_\nu^\infty \gg L_\gamma^\infty$.

In the case (i) one has a simple $L_\gamma^\infty - \langle \dot{M} \rangle$ relation

$$L_\gamma^\infty = L_{\text{DCH}}^{(0)} \langle \dot{M}_{10} \rangle \sqrt{1 - x_g}. \quad (24)$$

It slightly depends on M and R due to General Relativity effects.

In the case (ii) the relation between L_γ^∞ and $\langle \dot{M} \rangle$ is more complicated. One can use the approximations (20) to derive $L_\gamma^\infty(\langle \dot{M} \rangle, M, R)$ analytically for the three neutrino emission mechanisms, nn-bremsstrahlung in the SF case; MU or DU processes in the non-SF case (Section 4.2). Then the neutron star thermal equilibrium reads

$$L_{\text{DCH}}^{(0)} \langle \dot{M}_{10} \rangle \sqrt{1 - x_g} = Q_0 R^3 J_{kp}(M, R) \tilde{T}_9^n; \quad (25)$$

Q_0 , n , k and p are listed in Table 2 for each neutrino emission scenario. To calculate L_γ^∞ one needs to relate T_s and \tilde{T} . This can be done using the $T_s - T_b$ relations derived by Potekhin et al. (2003), where T_b is the temperature at the bottom of the neutron star heat blanketing envelope. Making use of $T_b \sqrt{1 - x_g} = \tilde{T}$ and equation (25), we obtain

$$T_{b9} = (1 - x_g)^{\frac{1-n}{2n}} \left(\frac{L_{\text{DCH}}^{(0)} \langle \dot{M}_{10} \rangle}{Q_0 R^3 J_{kp}(M, R)} \right)^{1/n}. \quad (26)$$

The $T_s - T_b$ relations are sensitive to the chemical composition of the heat blanketing envelope which is rather uncertain and depends on details of nuclear burning in the envelope. The envelope

Table 3. Accreting neutron stars in XRTs whose surface thermal emission in quasi-stationary quiescent states has been detected/constrained as plotted on the right-hand panel of Fig. 5.

Num.	Source	Num.	Source
1	4U 1608–522	13	NGC 6440 X-1
2	Aql X-1	14	SAX J1810.8–2609
3	4U 1730–22	15	MXB 1659–29
4	RX J1709–2639	16	IGR 00291+5934
5	Terzan 5	17	XTE J1814–338
6	4U 2129+47	18	XTE J2123–058
7	1M 1716–315	19	XTE J1807–294
8	Terzan 1	20	XTE J0929–314
9	2S 1803–45	21	EXO 1747–214
10	KS 1731–260	22	NGC 6440 X-2
11	Cen X-4	23	1H 1905+000
12	XTE J1751–305	24	SAX J1808.4–3658

can be almost purely iron if all the accreted material has burnt to iron during an active XRT state. Alternatively, it can be almost fully accreted or intermediate if the burning in the envelope is slower. We consider the two limiting cases, the case of non-accreted iron (Fe) envelope and the case of fully accreted (acc) envelope. We denote the corresponding relations as $T_s(T_b; M, R, j)$. Using equation (22) we have

$$L_\gamma^\infty = 4\pi\sigma R^2 (1 - x_g) T_s^4(T_b; M, R, j), \quad (27)$$

where j = ‘acc’ or ‘Fe’ while T_b is given by equation (26).

5.2 Model-independent analysis of thermal states

The approximations (20) and (21) greatly simplify an analysis of thermal states of neutron stars in XRTs. Now we need only mass M , radius R , the neutrino emission scenario and the heat blanketing envelope type to calculate an $L_\gamma^\infty - \langle \dot{M} \rangle$ relation.

The left-hand panel of Fig. 5 shows six families of $L_\gamma^\infty - M$ curves for a fixed time-averaged mass accretion rate $\langle \dot{M} \rangle = 10^{-10} \text{ M}_\odot \text{ yr}^{-1}$. The families are for the three scenarios of neutrino emission (nn, MU, DU) and the two limiting models of neutron star heat blanketing envelopes (Fe and acc). The curves of different types are calculated from (27) for the different EOSs (Table 1) using the appropriate $M - R$ relations (Fig. 1). The six horizontal shaded bands enclose the curves of these six families. Recall that the DU curves are plotted only at $M \geq 1.5 \text{ M}_\odot$, moreover, even at $M \gtrsim 1.5 \text{ M}_\odot$ the DU curves are only underestimations of $L_\gamma^\infty - \langle \dot{M} \rangle$ relations, as our approximations overestimate $L_{\nu \text{ DU}}$. The presented bands can be treated as overestimated photon thermal luminosity bands for the DU curves. For each band, the bounding stellar models are chosen as $M = 2.05 \text{ M}_\odot$, $R = 9.90 \text{ km}$ (SLy; lower bound) and $M = 2.4 \text{ M}_\odot$, $R = 14.0 \text{ km}$ (NL3 $\omega\rho$; upper bound).

Note that the $L_\gamma^\infty - M$ relations are mostly non-monotonic. The luminosity increases with growing M for low-mass stars but then decreases again for massive stars; the lowest M does not necessarily correspond to the brightest source in the band. This is a consequence of General Relativity effects.

The right-hand panel of Fig. 5 shows the same six bands as on the left-hand panel, but in the $L_\gamma^\infty - \langle \dot{M} \rangle$ plane. Thin curves present numerical solutions of the initial equation (21) (without assuming $L_\nu^\infty \gg L_\gamma^\infty$) for the bounding neutron star models (see above). Such solutions almost coincide with the approximate ones

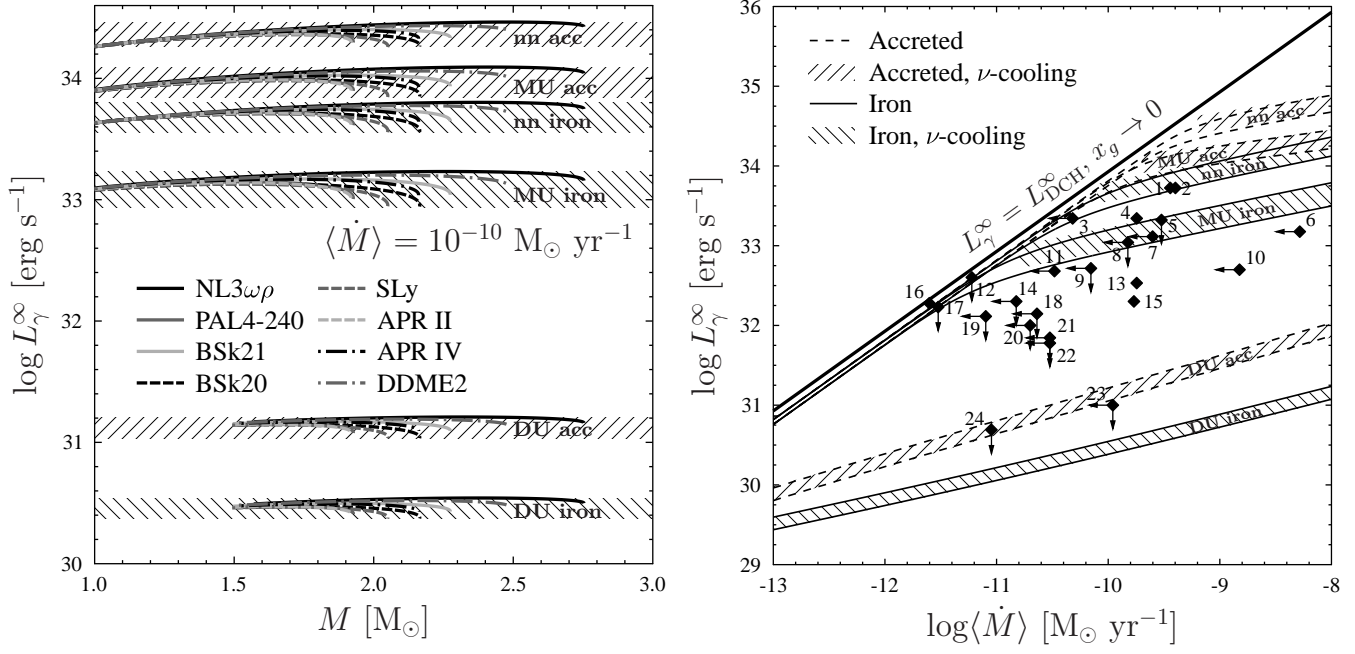


Figure 5. Left-hand panel: Six families of $L_\gamma^\infty - M$ relations for neutron stars in quiescent states of XRTs with a fixed averaged mass accretion rate $\langle \dot{M} \rangle = 10^{-10} M_\odot \text{ yr}^{-1}$. The families are specified by the neutrino emission mechanism (nn, MU or DU) and the composition of the envelope (Fe or acc). The lines of different types are calculated from equation (27) for the different EOSs. The shaded bands enclose these lines. Right-hand panel: 24 observed sources (Table 3) in the $L_\gamma^\infty - \langle \dot{M} \rangle$ plane. The bands are the same as on the left-hand panel. Thin curves restrict numerical solutions of equation (21) for the same six families. See the text for details.

if $L_\gamma^\infty \lesssim 0.1 L_{\text{DCH}}^\infty$. We stress that Fig. 5 illustrates only six representative scenarios of thermal states of neutron stars. Any filled band limits possible values of L_γ^∞ versus M or $\langle \dot{M} \rangle$ for neutron stars with the selected EOSs. Although the set of these EOSs is restricted we expect that the bands are robust (should not be greatly changed for a wider class of EOSs of nucleon matter). Another important feature is that the direct effect of the EOS on thermal states of neutron stars in XRTs for any of the six scenarios does not seem very strong. Therefore, the analysis of these scenarios is relatively model-independent.

Note also that the thin theoretical curves are valid only at $\langle \dot{M} \rangle \lesssim 10^{-9} M_\odot \text{ yr}^{-1}$. At higher accretion rates the internal thermal equilibrium of the neutron star is violated. This leads to higher L_γ^∞ than predicted by isothermal calculations.

The theoretical bands on the right-hand panel of Fig. 5 are compared with observational data (or observational upper limits shown by arrows) for 24 sources. The data are the same as those presented by Beznogov & Yakovlev (2015a,b) (who gave also the list of original publications). The sources are numbered in accordance with Table 3. They are mainly located between the MU and DU-cooling bands. Note the absence of any source with measured $\langle \dot{M} \rangle > 10^{-9} M_\odot \text{ yr}^{-1}$ except for 4U 2129+47 (source 6) and KS 1731–260 (source 10), for which only $\langle \dot{M} \rangle$ upper limits are given.

The thick solid black line on the right-hand panel of Fig. 5 corresponds to $L_\gamma = L_{\text{DCH}}$ (for non-redshifted quantities, $x_g \rightarrow 0$). It is the absolute upper bound on the thermal quiescent luminosity of a neutron star in the deep crustal heating scenario. One can see that all the data satisfy this upper bound. Actually, the data agree also with the highest ‘nn acc’ band and even with lower ‘MU acc’ or ‘nn iron’ bands, but disagree with the ‘MU iron’ band. This means that all the hottest neutron stars observed in quiescent states of XRTs

cannot be explained by the standard MU neutrino cooling and the standard iron envelopes. One needs either a slower (nn) neutrino cooling (strong SF) and/or accreted envelopes to raise L_γ^∞ and explain the data. The possibility of raising L_γ^∞ by strong SF has been analysed earlier (e.g., Yakovlev & Pethick 2004).

While the direct effects of EOS on thermal states of neutron stars in XRTs are not strong, other factors are seen (Fig. 5) to affect these thermal states much stronger. For instance, fixing the neutrino emission scenario (nn, MU or DU) but varying chemical composition of the heat blanketing envelope from pure iron to pure accreted can produce much stronger variations of L_γ^∞ (much wider bands) than those due to the EOSs. Alternatively, fixing the envelope composition (Fe or acc) and varying the neutrino emission scenarios (from nn to MU by proton superfluidity and to DU either by superfluidity or by nuclear physics effects, which shift M_{DU}), one can produce even stronger variations of L_γ^∞ .

Recall that in the strong neutrino emission (DU) scenario we have artificially extended the operation of the DU process over the entire neutron star core overestimating $L_{\nu\text{DU}}^\infty$ in massive stars. Accordingly, our DU bands in Fig. 5 appear to be downshifted by a factor of few with respect to the heating curves calculated in the previous analyses (e.g., Yakovlev et al. 2003; Levenfish & Haensel 2007; Beznogov & Yakovlev 2015a,b). Therefore, one should be careful in using our DU bands for analysing thermal states of the coldest sources, 1H 1905+000 (Jonker et al. 2006, 2007; Heinke et al. 2009) and SAX J1808.4–3658 (Heinke et al. 2007; Tomsick et al. 2005; Jonker et al. 2004) as massive neutron stars with the DU process on. These sources are very important for proving (or disproving) the operation of the DU process in massive stars. The real DU bands should lie by a factor of ~ 3 higher (in natural scale). However, we believe that our current DU bands have realistic widths and reasonably well describe variations of L_γ^∞ due

to composition of the envelopes. We expect to improve our model-independent analysis of the DU bands in our future publication.

6 DISCUSSION AND CONCLUSIONS

We have considered a representative set of seven EOSs for neutron stars with nucleon cores (Table 1) and analysed the models of neutron stars with isothermal interiors (with constant redshifted internal temperatures \tilde{T}). We have calculated the neutrino luminosities L_ν^∞ and heat capacities C_{core} of the cores of these stars with masses $M = 1.1 M_\odot, 1.2 M_\odot, \dots, M_{\text{max}}$ for several important scenarios of neutron star internal structure. The quantities L_ν^∞ and C_{core} almost coincide with the total neutrino luminosities and heat capacities of neutron stars.

Specifically, we have studied the three scenarios for L_ν^∞ which correspond to (i) the neutrino-pair bremsstrahlung in nn collisions (owing to the presence of strong proton superfluidity in the core); (ii) non-SF stars which cool via MU processes; (iii) non-SF stars cooling via powerful DU processes. We have considered the two scenarios for C_{core} , relevant for non-SF cores and the cores with strong proton superfluidity. The calculated values of L_ν^∞ and C_{core} have been accurately fitted by the analytic expressions (20) which are universal for all selected EOSs. The fit parameters (Table 2) are almost independent of the specific EOS. We expect that L_ν^∞ and C_{core} calculated for neutron stars with other EOSs of nucleon matter would be similar and could be approximated in the same way making our approximations almost model independent.

In this sense our consideration extends model-independent analysis of cooling neutron stars based on the standard neutrino cooling function $\ell(\tilde{T}) = L_{\nu\text{MU}}^\infty(\tilde{T})/C_{\text{core}}^{\text{non-SF}}(\tilde{T})$ (Yakovlev et al. 2011; Weisskopf et al. 2011; Klochov et al. 2015; Ofengeim et al. 2015). Ofengeim et al. (2015) derived also model-independent approximations to the neutrino cooling function $\ell(\tilde{T}) = L_{\nu\text{nn}}^\infty(\tilde{T})/C_{\text{core}}^{\text{SF}}(\tilde{T})$ for stars with strong proton superfluidity. Shternin & Yakovlev (2015) performed a more complicated model-independent analysis of the cooling enhanced by the onset of triplet-state pairing of neutrons and associated neutrino emission in neutron star cores.

Our present results are more refined because we analyse a weak dependence of L_ν^∞ and C_{core} on the EOS. Our approximations of L_ν^∞ and C_{core} greatly simplify calculations of cooling of isolated neutron stars at the neutrino cooling stage after the initial thermal relaxation ($100 \lesssim t \lesssim 10^5$ yr). This cooling is governed by the neutrino cooling function $\ell = L_\nu^\infty/C_{\text{core}}$. The expressions for ℓ obtained from our fits of L_ν^∞ and C_{core} are in good agreement with the approximations used in Yakovlev et al. (2011); Weisskopf et al. (2011); Klochov et al. (2015); Ofengeim et al. (2015) but ours seem more complete. The approximations of C_{core} should simplify cooling simulations of isolated neutron stars at the photon cooling stage (at $t \gtrsim 10^5$ yr, when the neutrino luminosity L_ν^∞ becomes unimportant). Finally, the approximations we obtained for L_ν^∞ simplify considerations of thermal states of accreting neutron stars in quasi-stationary XRTs as demonstrated in Section 5.

Let us stress that our results are far from being perfect because they are obtained under a number of simplified assumptions. For instance, while constructing the approximations we have assumed the ratio $R_{\text{core}}/R \approx 0.9$ to be constant. In fact, it slightly decreases with the growth of M . It may be so that one can improve our fits taking into account the approximations of R_{core}/R by Zdunik et al. (2016).

While approximating $L_{\nu\text{DU}}^\infty$ we have assumed that the DU pro-

cess is open in the entire core. In fact, it can operate in a small central kernel. The size of this kernel depends on M and the EOS model. Its radius is zero at $M = M_{\text{DU}}$ but increases with growing M . Moreover, according to Table 1, for three of the seven selected EOSs the DU process is forbidden in all stable neutron star models. Thus, our approximation of $L_{\nu\text{DU}}^\infty$ can be treated as an overestimation to be improved in the future.

We have considered superfluidity of nucleons in a simplified manner, i.e. we have assumed that neutrons are totally non-superfluid but protons are either totally non-superfluid or fully superfluid. The advantages and disadvantages of such a treatment are discussed by Ofengeim et al. (2015).

Another simplification of our approach is in using constant effective nucleon masses equal to 0.7 of their bare masses. In addition, the neutrino emissivities have been calculated employing approximate squared matrix elements of neutrino reactions taken by Yakovlev et al. (2001) from calculations by Friman & Maxwell (1979). We expect that we can include a more advanced physics using a similar formalism when this physics appears for a number of representative EOSs.

ACKNOWLEDGEMENTS

The work of DG was supported partly by the RFBR (grants 14-02-00868-a and 16-29-13009-ofi-m) and the work of PH, LZ and MF by the Polish NCN research grant no. 2013/11/B/ST9/04528. One of the authors (DDO) is grateful to N. Copernicus Astronomical Center for hospitality and perfect working conditions.

REFERENCES

- Antoniadis J., Freire P. C. C., Wex N., Tauris T. M., Lynch R. S., van Kerkwijk M. H., et al. 2013, *Science*, 340, 448
- Beznogov M. V., Yakovlev D. G., 2015a, *MNRAS*, 447, 1598
- Beznogov M. V., Yakovlev D. G., 2015b, *MNRAS*, 452, 540
- Brown E. F., Bildsten L., Rutledge R. E., 1998, *Atrophys. J. Lett.*, 504, L95
- Degenaar N., Wijnands R., Bahramian A., Sivakoff G. R., Heinke C. O., Brown E. F., Fridriksson J. K., Homan J., Cackett E. M., Cumming A., Miller J. M., Altamirano D., Pooley D., 2015, *MNRAS*, 451, 2071
- Demorest P. B., Pennucci T., Ransom S. M., Roberts M. S. E., Hessels J. W. T., 2010, *Nature*, 467, 1081
- Douchin F., Haensel P., 2001, *Astron. Astrophys.*, 380, 151
- Fortin M., Providencia C., Raduta A. R., Gulminelli F., Zdunik J. L., Haensel P., Bejger M., 2016, *ArXiv e-prints*
- Friman B. L., Maxwell O. V., 1979, *Astrophys. J.*, 232, 541
- Glen G., Sutherland P., 1980, *Astrophys. J.*, 239, 671
- Gudmundsson E. H., Pethick C. J., Epstein R. I., 1983, *Astrophys. J.*, 272, 286
- Gusakov M. E., Kaminker A. D., Yakovlev D. G., Gneden O. Y., 2005, *MNRAS*, 363, 555
- Haensel P., Potekhin A. Y., Yakovlev D. G., 2007, *Neutron Stars. 1. Equation of State and Structure*. Springer, New York
- Haensel P., Zdunik J. L., 1990, *Astron. Astrophys.*, 227, 431
- Haensel P., Zdunik J. L., 2003, *Astron. Astrophys.*, 404, L33
- Haensel P., Zdunik J. L., 2008, *Astron. Astrophys.*, 480, 459
- Heinke C. O., Jonker P. G., Wijnands R., Deloye C. J., Taam R. E., 2009, *Astrophys. J.*, 691, 1035

- Heinke C. O., Jonker P. G., Wijnands R., Taam R. E., 2007, *Astrophys. J.*, 660, 1424
- Jonker P. G., Bassa C. G., Nelemans G., Juett A. M., Brown E. F., Chakrabarty D., 2006, *MNRAS*, 368, 1803
- Jonker P. G., Steeghs D., Chakrabarty D., Juett A. M., 2007, *Astrophys. J. Lett.*, 665, L147
- Jonker P. G., Wijnands R., van der Klis M., 2004, *MNRAS*, 349, 94
- Kaminker A. D., Kaurov A. A., Potekhin A. Y., Yakovlev D. G., 2014, *MNRAS*, 442, 3484
- Kaminker A. D., Yakovlev D. G., Haensel P., 2016, *Astrophys. Sp. Sci.*, 361, 267
- Klochkov D., Suleimanov V., Pühlhofer G., Yakovlev D. G., Santangelo A., Werner K., 2015, *Astron. Astrophys.*, 573, A53
- Lattimer J. M., Pethick C. J., Prakash M., Haensel P., 1991, *Physical Review Letters*, 66, 2701
- Lattimer J. M., Prakash M., 2001, *Astrophys. J.*, 550, 426
- Levenfish K. P., Haensel P., 2007, *Astrophys. Sp. Sci.*, 308, 457
- Ofengeim D. D., Kaminker A. D., Klochkov D., Suleimanov V., Yakovlev D. G., 2015, *MNRAS*, 454, 2668
- Page D., 1993, in Guidry M. W., Strayer M. R., eds, *Nuclear Physics in the Universe The Geminga neutron star: Evidence for nucleon superfluidity at very high density*. pp 151–162
- Page D., Applegate J. H., 1992, *Astrophys. J. Lett.*, 394, L17
- Page D., Lattimer J. M., Prakash M., Steiner A. W., 2009, *Astrophys. J.*, 707, 1131
- Potekhin A. Y., Chabrier G., Yakovlev D. G., 1997, *Astron. Astrophys.*, 323, 415
- Potekhin A. Y., Fantina A. F., Chamel N., Pearson J. M., Goriely S., 2013, *Astron. Astrophys.*, 560, A48
- Potekhin A. Y., Pons J. A., Page D., 2015, *Space Sci. Rev.*, 191, 239
- Potekhin A. Y., Yakovlev D. G., Chabrier G., Gnedin O. Y., 2003, *Astrophys. J.*, 594, 404
- Shapiro S. L., Teukolsky S. A., 1983, *Black holes, white dwarfs, and neutron stars: The physics of compact objects*. Wiley-Interscience, New York
- Shternin P. S., Yakovlev D. G., 2015, *MNRAS*, 446, 3621
- Tomsick J. A., Gelino D. M., Kaaret P., 2005, *Astrophys. J.*, 635, 1233
- Weisskopf M. C., Tennant A. F., Yakovlev D. G., Harding A., Zavlin V. E., O'Dell S. L., Elsner R. F., Becker W., 2011, *Astrophys. J.*, 743, 139
- Yakovlev D. G., Haensel P., 2003, *Astron. Astrophys.*, 407, 259
- Yakovlev D. G., Ho W. C. G., Shternin P. S., Heinke C. O., Potekhin A. Y., 2011, *MNRAS*, 411, 1977
- Yakovlev D. G., Kaminker A. D., Gnedin O. Y., Haensel P., 2001, *Phys. Rep.*, 354, 1
- Yakovlev D. G., Levenfish K. P., Haensel P., 2003, *Astron. Astrophys.*, 407, 265
- Yakovlev D. G., Pethick C. J., 2004, *Annu. Rev. Astron. Astrophys.*, 42, 169
- Zdunik J. L., Fortin M., Haensel P., 2016, *in prep.*, *Astron. Astrophys.*